EXACT CALCULATION OF THE PENETRABILITY FOR A SIMPLE TWO-DIMENSTIONAL HEAVY-ION FUSION BARRIER*

T. Kodama and R. A. M. S. Nazareth
Centro Brasileiro de Pesquisas Físicas, Rio de Janeiro, Brazil

P. Möller† and J. R. Nix
Theoretical Division, Los Alamos Scientific Laboratory
University of California, Los Alamos, New Mexico 87545

ABSTRACT

In a study of the effect of the quantal zero-point oscillations of nuclei on their low-energy fusion cross section, we calculate exactly the penetrability for a simple two-dimensional barrier $V(r,c)$. The coordinate r is the distance between the centers of mass of the two nuclei, and σ is the sum of the root-mean-square extensions along the symmetry axis of the mass of each nucleus about its center of mass. The potential $V(r,\sigma)$ is a parabolic peak in r and is one or the other of two harmonic oscillators in σ, depending upon whether r is greater than or less than a critical value r_1. The oscillators differ both in the locations of their

minima and in their curvatures. This simulates the dominant feature in the two-dimensional nuclear potential-energy surface of two misaligned valleys (the fission and fusion valleys) separated by a ridge between them. When an incident wave that is localized in the fusion valley encounters the potential-energy ridge, it is partially transmitted and partially reflected in waves that correspond to different excited states in the transverse direction and hence to different amounts of energy in the fusion direction. The amplitudes of these waves are determined by requiring that the wave functions (expressed exactly in terms of parabolic-cylinder functions) and their first derivatives be continuous at r_1. The penetrability is then obtained from the amplitudes of the transmitted waves. As a specific example, we use this formalism to calculate the penetrability for a two-dimensional potential-energy surface appropriate to the reaction $^{100}Mo + {}^{100}Mo \rightarrow {}^{200}Po$. The calculated penetrability is substantially different from the result for a one-dimensional calculation. In particular, 10 MeV below the maximum in the one-dimensional fusion barrier the two-dimensional penetrability is 10^{10} times as large as the one-dimensional result. Also, for equal penetrability the slopes of the two curves are very different.

[NUCLEAR REACTIONS, HEAVY-ION $^{100}Mo + {}^{100}Mo \rightarrow {}^{200}Po$. Calculated exactly penetrability for simple two-dimensional fusion barrier. Heavy-ion fusion cross section, multidimensional-barrier penetration, parabolic-cylinder functions.]

I. INTRODUCTION

The goal of many experiments in heavy-ion physics is to provide information on the nuclear potential energy of deformation. In particular, the measurement of heavy-ion fusion cross sections at low bombarding energies provides information on the height of the interaction barrier and on its curvature near the point where the two nuclei first come into contact. These quantities are usually extracted by analyzing the experimental fusion cross section in terms of the penetrability for a one-dimensional interaction barrier. The shape of this barrier is often assumed to be parabolic, which leads to a simple analytic expression for the penetrability.[1-4] If the target or projectile is deformed in its ground state, the height of the interaction barrier depends upon the angular orientation of the deformed nucleus. This effect is usually taken into account by averaging over orientation[4-6] or in some other way.[7]

Such procedures are fair approximations in the case of a relatively light incident projectile, where the nuclear potential energy depends primarily upon a single coordinate that describes the distance between the centers of mass of the two nuclei. However, as the mass of the projectile increases, it becomes increasingly important to take into account the possibility that the nuclei may deform during the collision. In particular, near the point at which the nuclei first come into contact, the potential energy depends strongly upon the distance between their equivalent sharp nuclear surfaces. For a fixed separation of their centers of mass, this distance is related to the sum of their deformations along a common symmetry axis. Prolate deformations lower the potential energy relative to that for two spheres, whereas oblate deformations raise it. In terms of a center-of-mass separation coordinate r and a fragment-

elongation coordinate σ, the two-dimensional potential-energy surface $V(r,\sigma)$ has the appearance of two misaligned valleys--one associated with fission and the other with fusion--separated by a ridge between them.[8-13] This is illustrated[13] in Fig. 1 for the reaction $^{100}Mo + {}^{100}Mo \rightarrow {}^{200}Po$.

It has been recognized for several years that nuclei can deform during heavy-ion collisions, and classical dynamical calculations have been performed to describe the deformation of nuclei both before they come into contact[14-21] and after contact.[12,22-26] However, for energies near or below the top of the one-dimensional interaction barrier, classical mechanics is no longer valid. For these energies it is necessary to use a quantal approach in describing the collision.

Within the collective model of the nucleus, the full solution of the quantal collision problem would require solving a multidimensional Schrödinger equation in terms of the coordinates that describe the shapes and angular orientations of the two colliding nuclei. We do not solve this multidimensional problem here, but instead calculate the penetrability for a restricted two-dimensional problem, taking into account only a center-of-mass separation coordinate and a fragment-elongation coordinate.

When the two nuclei are far apart, the ground-state wave function for the motion perpendicular to the fusion valley is approximately a Gaussian function centered about the bottom of the valley. The width of this function, which regulates the amplitude of the zero-point oscillations, is determined by the curvature of the potential energy perpendicular to the valley and by the associated effective mass.

During a heavy-ion fusion reaction, when an incident wave localized in this way in the fusion valley arrives in the vicinity of the potential-energy ridge and the fission valley, it is partially transmitted

and partially reflected in waves that correspond to different excited states in the transverse direction. This leads to a distribution in the amount of energy in the fusion direction that is available for penetrating the barrier. Those components with increased energy in the fusion direction penetrate more easily, which increases the penetrability. Because this is especially true for low incident energies, the resulting dependence of the penetrability on energy is qualitatively similar to that calculated for a one-dimensional barrier that is somewhat lower in height and substantially thinner.

The importance of calculating the penetrability for a two-dimensional barrier has long been recognized, and some advances have been made recently on this problem. Hofmann has applied the WKB approximation and the Born approximation to two-dimensional potentials of interest in fission.[27] Miller has developed a classical-limit treatment of quantum mechanics that involves solving classical equations of motion for complex time.[28] This method has been used by Massmann, Ring, and Rasmussen to calculate the penetrability through a simple two-dimensional fission barrier at energies well below the top of the barrier.[29,30] Unfortunately, the Born approximation that appears in Hofmann's treatment is poor when applied to a potential ridge, and Miller's method does not apply for incident energies near the top of the barrier, which is a region of great experimental interest.

We are therefore led to consider a two-dimensional potential which displays the salient feature of two misaligned valleys, but that is nevertheless sufficiently simple that an exact solution can be effected. Some preliminary accounts of our approach are given in Refs. 31 and 32.

II. POTENTIAL AND KINETIC ENERGIES

We represent the dependence of the potential energy on the separation coordinate in terms of a parabolic peak centered at the maximum in the one-dimensional interaction barrier, and represent the fission and fusion valleys in terms of two harmonic oscillators whose curvatures and equilibrium positions are different. To be specific, we approximate the two-dimensional potential-energy surface $V(r,\sigma)$ by

$$V(r,\sigma) = \begin{cases} V_0 - \frac{1}{2}k_r(r-r_0)^2 + \frac{1}{2}k_1(\sigma-\sigma_1)^2 & , r \geq r_1 \\ V_0 - \frac{1}{2}k_r(r-r_0)^2 + \frac{1}{2}k_2(\sigma-\sigma_2)^2 - \frac{1}{2}k_2(\sigma_2-\sigma_1)^2 & , r < r_1 \end{cases} . \quad (1)$$

The position of the peak in the separation coordinate is at $r = r_0$. The fusion valley is centered about $\sigma = \sigma_1$ and occurs for values of r greater than or equal to the critical value r_1. The fission valley is centered about $\sigma = \sigma_2$ and occurs for values of r less than r_1. The positive quantity k_r specifies the curvature with respect to r of the parabolic peak, and k_1 and k_2 specify the curvatures with respect to σ in the fusion and fission valleys, respectively. Along the one-dimensional path defined by $\sigma = \sigma_1$, the potential energy is continuous and has the maximum value V_0 at $r = r_0$. The energy of the fission saddle point, which occurs at $r = r_0$, $\sigma = \sigma_2$, is $V_0 - \frac{1}{2}k_2(\sigma_2 - \sigma_1)^2$.

This representation of the potential-energy surface is shown in the lower part of Fig. 2 for the reaction $^{100}Mo + {}^{100}Mo \rightarrow {}^{200}Po$. For comparison, the upper part of the figure shows the actual calculated macroscopic potential-energy surface for this reaction.[13] The eight constants appearing in Eq. (1) were selected to yield the correct energy

and location in both r and σ of the maximum in the one-dimensional interaction barrier, the correct energy and location in σ of the fission saddle point, the correct energy and location in r where stability with respect to σ deformations is lost in the fusion valley, and the correct curvature with respect to σ in the fusion valley. The energies in both the upper and lower parts of Fig. 2 are plotted relative to the maximum V_0 in the one-dimensional interaction barrier.

The kinetic energy T is taken to be

$$T = \begin{cases} \frac{1}{2} m_r \dot{r}^2 + \frac{1}{2} m_1 \dot{\sigma}^2 & , \quad r \geq r_1 \\ \frac{1}{2} m_r \dot{r}^2 + \frac{1}{2} m_2 \dot{\sigma}^2 & , \quad r < r_1 \end{cases} ,$$

where the effective masses m_r, m_1, and m_2 are independent of position. The frequencies of oscillation in the fusion and fission valleys are therefore

$$\omega_1 = (k_1/m_1)^{1/2}$$

and

$$\omega_2 = (k_2/m_2)^{1/2} ,$$

respectively. The associated curvature parameter for the parabolic peak is

$$\omega_r = (k_r/m_r)^{1/2} .$$

For m_r we use the reduced mass of the two colliding nuclei, and for both m_1 and m_2 we use the incompressible, irrotational mass for vibrations about spherical equilibrium shapes in the fusion valley.[13] For the reaction $^{100}Mo + {}^{100}Mo \rightarrow {}^{200}Po$ this leads to the values

$$\hbar\omega_r = 2.61 \text{ MeV} ,$$

$$\hbar\omega_1 = 3.29 \text{ MeV} ,$$

and

$$\hbar\omega_2 = 4.25 \text{ MeV}.$$

When the bombarding energy is measured relative to the maximum V_0 in the one-dimensional interaction barrier, the penetrability depends upon only two additional quantities, whose values for this reaction are

$$r_1 - r_0 = 1.56 \text{ fm}$$

and

$$\sigma_2 - \sigma_1 = 1.45 \text{ fm}.$$

III. PENETRABILITY

Because of the forms chosen for the potential and kinetic energies, the total wave function $\Psi(r,\sigma)$ is given exactly in each of the two regions in terms of a sum of parabolic-cylinder functions in r times harmonic-oscillator wave functions in σ. The boundary conditions that we are interested in correspond to an incident wave in the ground state in the fusion valley travelling toward the left from $r = +\infty$ and to a sum of transmitted and reflected waves. The transmitted waves correspond to exciting different harmonic-oscillator states in the fission valley and travel asymptotically toward $r = -\infty$. The reflected waves correspond to exciting different harmonic-oscillator states in the fusion valley and travel asymptotically toward $r = +\infty$.

The wave function in the fusion-valley is therefore given by

$$\Psi_1(r,\sigma) = E^*(a_{10},u)\,\psi_{10}(\sigma-\sigma_1) + \sum_{n=0}^{\infty} A_n\, E(a_{1n},u)\;\; \psi_{1n}(\sigma-\sigma_1)\;\;,$$

where the parabolic-cylinder functions E and E^* are solutions in standard notation[33,34] of the differential equation

$$\frac{d^2\phi}{du^2} + \left(\frac{1}{4}u^2 - a\right)\phi = 0.$$

Complex conjugation is denoted by an asterisk. The dimensionless variable u that appears in these functions is related to r by

$$u = (2m_r\omega_r/\hbar)^{1/2}\;\; (r-r_0) = \left[2k_r/(\hbar\omega_r)\right]^{1/2}(r-r_0).$$

The quantity a_{1n} is given by

$$a_{1n} = \left[V_0 - (E - n\hbar\omega_1)\right]\;\; /(\hbar\omega_1)$$

and specifies in units of $\hbar\omega_r$ the energy deficit relative to V_0 for motion in the r direction when the n-th harmonic-oscillator state in the fusion valley is excited. The total energy of the system E (not to be confused with the parabolic-cylinder functions denoted by the same symbol) includes the zero-point energy $\frac{1}{2}\hbar\omega_1$. The properly normalized harmonic-oscillator wave functions in the fusion valley are given by

$$\psi_{1n}(\sigma-\sigma_1) = \left[\alpha_1/(2^n n!\sqrt{\pi})\right]^{1/2}\;\; H_n\left[\alpha_1(\sigma-\sigma_1)\right]\exp\left[-\tfrac{1}{2}\alpha_1{}^2(\sigma-\sigma_1)^2\right], \quad (2)$$

where

$$\alpha_1 = (m_1\omega_1/\hbar)^{1/2} = \;\; k_1/(\hbar\omega_1)^{\;\;1/2}$$

and where H_n denotes the n-th Hermite polynomial.

Similarly, the wave function in the fission valley is given by

$$\Psi_2(r,\sigma) = \sum_{n=0}^{\infty} B_n E(a_{2n}, -u)\, \psi_{2n}(\sigma-\sigma_2) \quad ,$$

where

$$a_{2n} = \left\{ V_0 - \tfrac{1}{2} k_2(\sigma_2 - \sigma_1)^2 - \left[E + \tfrac{1}{2}\hbar\omega_1 - (n + \tfrac{1}{2})\hbar\omega_2 \right] \right\} / (\hbar\omega_r)$$

and where the harmonic-oscillator wave functions are given by expressions analogous to Eqs. (2) and (3).

The reflection and transmission coefficients A_n and B_n are determined by requiring that the wave function and its gradient be continuous at r_1 for all values of σ. The resulting two equations are transformed into two systems of algebraic equations by multiplying by $\psi^*_{1m}(\sigma-\sigma_1)$ and integrating over all values of σ. This leads to

$$E^*(a_{10},u_1)\,\delta_{m0} + E(a_{1m},u_1)A_m = \sum_{n=0}^{\infty} c_{mn}\, E(a_{2n}, -u_1)\, B_n \quad ,$$

E on line

$$E^{*\prime}(a_{10},u_1)\,\delta_{m0} + E'(a_{1m},u_1)A^m = \sum_{n=0}^{\infty} c_{mn}\, E'(a_{2n}, -u_1)B_n \quad ,$$

where the primes denote differentiation with respect to u and where

$$c_{mn} = \int_{-\infty}^{+\infty} \psi^*_{1m}(\sigma-\sigma_1)\psi_{2n}(\sigma-\sigma_2)\,d\sigma \quad . \tag{4}$$

Elimination of A_m from these equations leads to

$$\left[E(a_{1m},u_1)E^{*\prime}(a_{10},u_1) - E^{\prime}(a_{1m},u_1)E^{*}(a_{10},u_1) \right] \delta_{m0} =$$

$$\sum_{n=0}^{\infty} c_{mn} \left[E(a_{1m},u_1)E^{\prime}(a_{2n},-u_1) - E^{\prime}(a_{1m},u_1)E(a_{2n},-u_1) \right] B_n \quad .$$

The presence of the kronecker delta in the left-hand side of this equation permits us to use the Wronskian property[33,34]

$$W\left[E(a,u),\ E^{*}(a,u) \right] = -2i.$$

In terms of the matrix M defined by

$$M_{mn} = \frac{1}{2} i c_{mn} W\left[E(a_{1m},u_1),\ E(a_{2n},-u_1) \right] \quad ,$$

the system of equations to be solved for the coefficients B_n becomes simply

$$\sum_{n=0}^{\infty} M_{mn} B_n = \delta_{m0} \quad .$$

The expansion coefficients c_{mn} are obtained conveniently by multiplying both sides of Eq. (4) by $x^m y^n/(m!n!)$ and summing on m and n from 0 to ∞, which permits the use of the Hermite-polynomial generating function to evaluate the integral. Subsequent use of the generating function returns the right-hand side of the equation to a summation, and the value of c_{mn} is determined by equating the coefficients of $x^m y^n$. This leads to

$$c_{mn} = \left[\frac{m!n!\alpha_1\alpha_2}{2^{m+n-1}(\alpha_1^2+\alpha_2^2)}\right]^{1/2}\left(\frac{\alpha_2^2-\alpha_1^2}{\alpha_1^2+\alpha_2^2}\right)^{(m+n)/2}\exp\left[-\frac{\alpha_1^2\alpha_2^2(\sigma_2-\sigma_1)^2}{2(\alpha_1^2+\alpha_2^2)}\right]$$

$$\times \sum_{k=0}^{\min(m,n)} \frac{1}{k!(m-k)!(n-k)!}\left(\frac{4\alpha_1\alpha_2}{\alpha_2^2-\alpha_1^2}\right)^k H_{m-k}\left[\frac{\alpha_1\alpha_2^2(\sigma_2-\sigma_1)}{(\alpha_2^4-\alpha_1^4)^{1/2}}\right]$$

$$\times \bar{H}_{n-k}\left[-\frac{\alpha_1^2\alpha_2(\sigma_2-\sigma_1)}{(\alpha_2^4-\alpha_1^4)^{1/2}}\right] ,$$

where we specialize to the physically interesting case in which $\alpha_2 > \alpha_1$ and where

$$\bar{H}_n(x) = (-i)^n H_n(ix) \quad .$$

The penetrability P is obtained by taking the ratio of the transmitted flux to the incident flux, integrated over all values of σ. By virtue of Eq. (5) the final expression for P becomes

$$P = \sum_{n=0}^{\infty} |B_n|^2 = \sum_{n=0}^{\infty} |(M^{-1})_{n0}|^2 = \left[(MM^{\dagger})^{-1}\right]_{00} ,$$

where $M^{\dagger}$ denotes the transposed complex-conjugate of M.

In the limiting case in which the fission and fusion valleys become coincident ($\sigma_1 = \sigma_2$, $k_1 = k_2$, and $m_1 = m_2$), the expansion coefficients c_{mn} are given simply by $c_{mn} = \delta_{mn}$. In this case the expression for the penetrability reduces to the usual Hill-Wheeler formula[1]

$$P = \left[1 + \exp(2\pi a_{10}) \right]^{-1} \quad ,$$

where

$$a_{10} = a_{20} = (V_0 - E) / (\hbar\omega_r) \quad .$$

When calculating the penetrability by use of the above formalism, one must take extreme care with the numerical procedures employed. This is especially true when calculating the parabolic-cylinder functions for moderately large values of the arguments, as significant loss of accuracy occurs through the subtraction of terms of comparable magnitude. In our calculations, we have used the standard power-series expansions for the parabolic-cylinder functions[33,34] and have overcome the numerical difficulties by performing the computations in double-precision arithmetic on a CDC 6600 computer, which yields a word length of approximately 28 decimal figures. If a computer with such precision is not available, or if the parabolic-cylinder functions are needed for other ranges of the arguments, then other methods must be used for computing them.[35] Also, one must insure that the calculated penetrability has converged as a function of basis size. In our calculations, we used 20 basis functions when $E - V_0 \leq -15$ MeV and 25 basis functions when $E - V_0 \geq -15$ MeV.

Figure 3 shows the calculated penetrability as a function of bombarding energy for a two-dimensional potential-energy surface appropriate to the reaction $^{100}Mo + {}^{100}Mo \rightarrow {}^{200}Po$. The penetrability for the two-dimensional barrier is substantially different from that for a corresponding one-dimensional parabolic barrier with the same height V_0 and same curvature $\hbar\omega_r$ as the two-dimensional barrier. At energies well below the maximum V_0 in the one-dimensional barrier, the penetrability

for the two dimensional barrier is substantially larger than that for the one-dimensional barrier. For example, 10 MeV below V_0 it is 10^{10} times as large. This increased penetrability arises because in the two-dimensional potential-energy surface increased fragment elongation leads to a decrease in potential energy near the maximum in the one-dimensional interaction barrier. At energies well above V_0 the penetrability for the two-dimensional barrier is less than that for the one-dimensional barrier. This arises because the discontinuity in the two-dimensional potential-energy surface at r_1 increases the reflection of the incident wave at high energies. Finally, for equal penetrability the slopes of the two curves are very different.

The resonances in the penetrability for the two-dimensional barrier arise because of the lake between the fission saddle point and the fusion valley that occurs in our approximation to the potential-energy surface; see again the lower part of Fig. 2. Because this lake is not present in the actual macroscopic potential-energy surface, the resonances would not occur for this case. However, single-particle effects could lead to small lakes in the total potential-energy surface, which would in turn give rise to small resonances in the penetrability.

IV. SUMMARY AND CONCLUSION

We have calculated exactly the penetrability for a simple two-dimensional potential-energy surface $V(r,\sigma)$, where r is the distance between the centers of mass of the two nuclei, and σ is a fragment-elongation coordinate. The potential is a parabolic peak in r and is one or the other of two harmonic oscillators in σ, depending upon whether r is

greater than or less than a critical value r_1. It reproduces correctly several features of the true macroscopic two-dimensional potential-energy surface, including the energy and location in both r and σ of the maximum in the one-dimensional interaction barrier, the energy and location in σ of the fission saddle point, the energy and location in r where stability with respect to σ deformations is lost in the fusion valley, and the correct curvature with respect to σ in the fusion valley.

For such a potential the total wave function $\Psi(r,\sigma)$ was written exactly in each of the two regions in terms of a sum of parabolic-cylinder functions in r times harmonic-oscillator wave functions in σ. The reflection and transmission coefficients were determined by requiring that the wave function and its gradient be continuous at r_1 for all values of σ. The penetrability was then obtained by taking the ratio of the transmitted flux to the incident flux, integrated over all values of σ.

With this formalism, we calculated the penetrability as a function of bombarding energy for a two-dimensional potential-energy surface appropriate to the reaction $^{100}Mo + {}^{100}Mo \rightarrow {}^{200}Po$. The calculated penetrability was found to be substantially different from the result calculated for a corresponding one-dimensional parabolic barrier. For example, 10 MeV below the maximum in the one-dimensional barrier, the penetrability for the two-dimensional barrier is 10^{10} times as large as that for the one-dimensional barrier. Also, for equal penetrability the slopes of the two curves are very different.

Previous analyses of heavy-ion fusion cross sections at low bombarding energies have taken into account the effect of the static nuclear ground-state deformations on the penetrability.[5-7] The results of the present study indicate that the penetrability is also affected by the

dependence of the potential energy upon fragment elongation near the maximum in the one-dimensional interaction barrier. We hope that future analyses of heavy-ion fusion cross sections at low bombarding energies will take into account the effect of the multidimensional potential-energy surface on the penetrability.

ACKNOWLEDGMENT

J. R. Nix thanks the Brazilian Nuclear Energy Commission for its financial support and the Centro Brasileiro de Pesquisas Físicas for its hospitality during the early phases of this work.

FOOTNOTES

*This work was supported by the Brazilian Nuclear Energy Commission and by the U.S. Energy Research and Development Administration.

†Present address: Department of Mathematical Physics, University of Lund, Lund 7, Sweden.

[1]D. L. Hill and J. A. Wheeler, Phys. Rev. 89, 1102 (1953).

[2]T.D. Thomas, Annu. Rev. Nucl. Sci. 18, 343 (1968).

[3]C. Y. Wong, Phys. Lett. 42B, 186 (1972).

[4]C. Y. Wong, Phys. Rev. Lett. 31, 766 (1973).

[5]W. Scobel, A. Mignerey, M. Blann, and H. H. Gutbrod, Phys. Rev. C 11, 1701 (1975).

[6]W. Scobel, H. H. Gutbrod, M. Blann, and A. Mignerey, Phys. Rev. C 14, 1808 (1976).

[7]L. C. Vaz and J. M. Alexander, Phys. Rev. C 10, 464 (1974).

[8]J. R. Nix and W. J. Swiatecki, Nucl. Phys. 71, 1 (1965).

[9]W. J. Swiatecki and S. Bjørnholm, Phys. Rep. 4C, 325 (1972).

[10]W. J. Swiatecki, J. Phys. Suppl. 33, C5-45 (1972).

[11]J. R. Nix, Annu. Rev. Nucl. Sci. 22, 65 (1972).

[12]J. R. Nix and A. J. Sierk, Phys. Scr. 10A, 94 (1974).

[13]P. Möller and J. R. Nix, Nucl. Phys. A272, 502 (1976).

[14]J. Maly and J. R. Nix, in Contributions to the International Conference on Nuclear Structure, Tokyo, Japan, 1967 [University of Tokyo report, 1967 (unpublished)] , p. 224.

[15]H. Holm, W. Scheid, and W. Greiner, Phys. Lett. 29B, 473 (1969).

[16]H. Holm, D. Scharnweber, W. Scheid, and W. Greiner, Z. Phys. 231, 450 (1970).

[17]H. Holm and W. Greiner, Phys. Rev. Lett. 24, 404 (1970).

[18]A. S. Jensen and C. Y. Wong, Phys. Rev. C 1, 1321 (1970).

[19]A. S. Jensen and C. Y. Wong, Nucl. Phys. A171, 1 (1971).

[20]P. W. Riesenfeldt and T. D. Thomas, Phys. Rev. C 2, 711 (1970).

[21]P. W. Riesenfeldt and T. D. Thomas, Phys. Rev. C 2, 2448 (1970).

[22]A. J. Sierk and J. R. Nix, in *Proceedings of the Third International Atomic Energy Agency Symposium on the Physics and Chemistry of Fission, Rochester, New York, 1973* (International Atomic Energy Agency, Vienna, 1974), Vol. II, p. 273.

[23]J. R. Nix and A. J. Sierk, in Proceedings of the International School-Seminar on Reactions of Heavy Ions with Nuclei and Synthesis of New Elements, Dubna, U.S.S.R., 1975 [Joint Institute for Nuclear Research Report No. JINR-D7-9734, 1976 (unpublished)], p. 101.

[24]A. J. Sierk and J. R. Nix, in Proceedings of the Symposium on Macroscopic Features of Heavy-Ion Collisions, Argonne, Illinois, 1976 [Argonne National Laboratory Report No. ANL/PHY-76-2, 1976 (unpublished)], Vol. I, p. 407.

[25]J. R. Nix and A. J. Sierk, Phys. Rev. C 15, 2072 (1977).

[26]A. J. Sierk and J. R. Nix, Phys. Rev. C (to be published).

[27]H. Hofmann, Nucl. Phys. A224, 166 (1974).

[28]W. M. Miller, Adv. Chem. Phys. 25, 69 (1974).

[29]H. Massmann, P. Ring, and J. O. Rasmussen, Phys. Lett. 57B, 417 (1975).

[30]P. Ring, J. O. Rasmussen, and H. Massmann, Fiz. Elem. Chastits At. Yad. 7, 916 (1976) [Sov. J. Part. Nucl. (to be published)].

[31]T. Kodma, R. A. M. S. Nazareth, and J. R. Nix, in Proceedings of the International Workshop III on Gross Properties of Nuclei and Nuclear Exitations, Hirschegg, Kleinwalsertal, Austria, 1975, edited by W. D. Myers [Technische Hochschule Darmstadt Report No. AED-Conf-75-009-000, 1975 (unpublished)], p. 146.

[32]T. Kodama, R. A. M. S. Nazareth, P. Möller, and J. R. Nix, in Contributions to the Meeting on Heavy-Ion Collisions, Fall Creek Falls State Park, Pikeville, Tennessee, 1977 [Oak Ridge National Laboratory report, 1977 (unpublished)].

[33]*Handbook of Mathematical Functions*, edited by M. Abramowitz and I. A. Stegun (National Bureau of Standards, Washington, D. C., 1964), pp. 692-695.

[34]J. C. P. Miller, in *Tables of Weber Parabolic Cylinder Functions* (Her Majesty's Stationery Office, London, 1955), pp. 80-89.

[35]H. Gräf, Lawrence Berkeley Laboratory Report No. LBL-2969, 1974 (unpublished).

FIGURE CAPTIONS

FIG. 1. Calculated[13] macroscopic two-dimensional potential-energy surface for the reaction $^{100}Mo + {}^{100}Mo \rightarrow {}^{200}Po$. The coordinate r is the distance between the centers of mass of the two nuclei, and σ is the sum of the root-mean-square extensions along the symmetry axis of the mass of each nucleus about its center of mass. The radius R_0 of the spherical nucleus is given by $R_0 = r_0 A^{1/3} = 1.16\ (200)^{1/3}$ fm = 6.78 fm. In this figure the zero of potential energy is at the sphere, whose location is given by a solid point. The location of two touching spheres is given by two adjacent solid points, and the location of the fission saddle point is given by two crossed solid lines.

FIG. 2. Comparison of calculated[13] macroscopic two-dimensional potential-energy surface (upper) and our approximation to it (lower) for the reaction $^{100}Mo + {}^{100}Mo \rightarrow {}^{200}Po$. In this figure the zero of potential energy is at the maximum in the one-dimensional interaction barrier, which is located at $r/R_0 = 1.64$, $\sigma/R_0 = 0.71$. This is slightly outside the configuration of two touching spheres, whose location is given by two adjacent solid points.

FIG. 3. Calculated penetrability for the reaction $^{100}Mo + {}^{100}Mo \rightarrow {}^{200}Po$ as a function of center-of-mass bombarding energy relative to the maximum in the one-dimensional interaction barrier. The solid curve gives the result for the two-dimensional barrier shown in the lower part of Fig. 2. As this curve is calculated at energy intervals of 0.25 MeV, the values at the resonances and local minima have limited precision. The dashed curve gives the result for a corresponding one-dimensional parabolic barrier with the same height and curvature as the two-dimensional barrier.

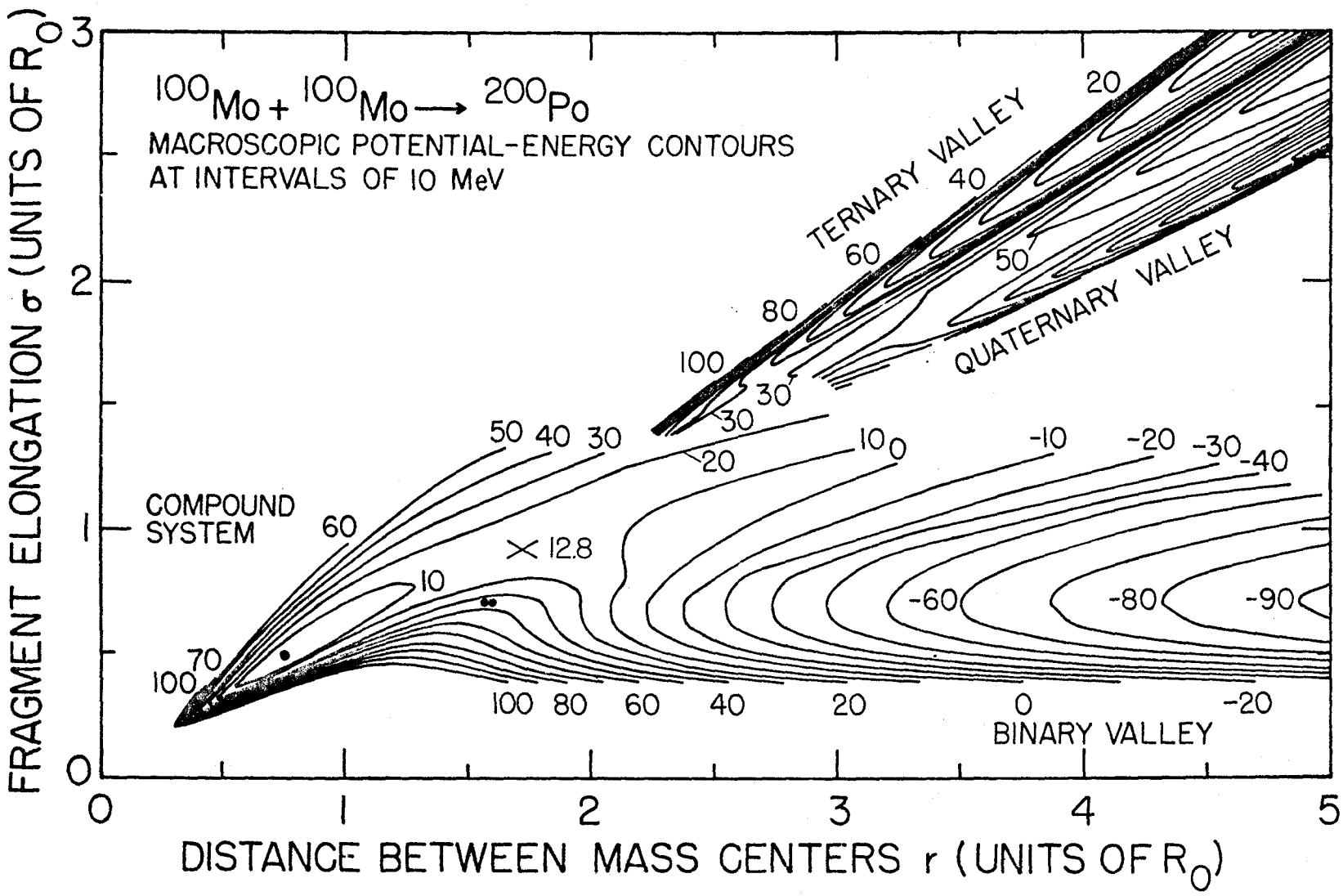
$^{100}Mo + {}^{100}Mo \longrightarrow {}^{200}Po$
MACROSCOPIC POTENTIAL-ENERGY CONTOURS
AT INTERVALS OF 10 MeV
TERNARY VALLEY
QUATERNARY VALLEY
COMPOUND SYSTEM
BINARY VALLEY
FRAGMENT ELONGATION σ (UNITS OF R_0)
DISTANCE BETWEEN MASS CENTERS r (UNITS OF R_0)

Figure 1

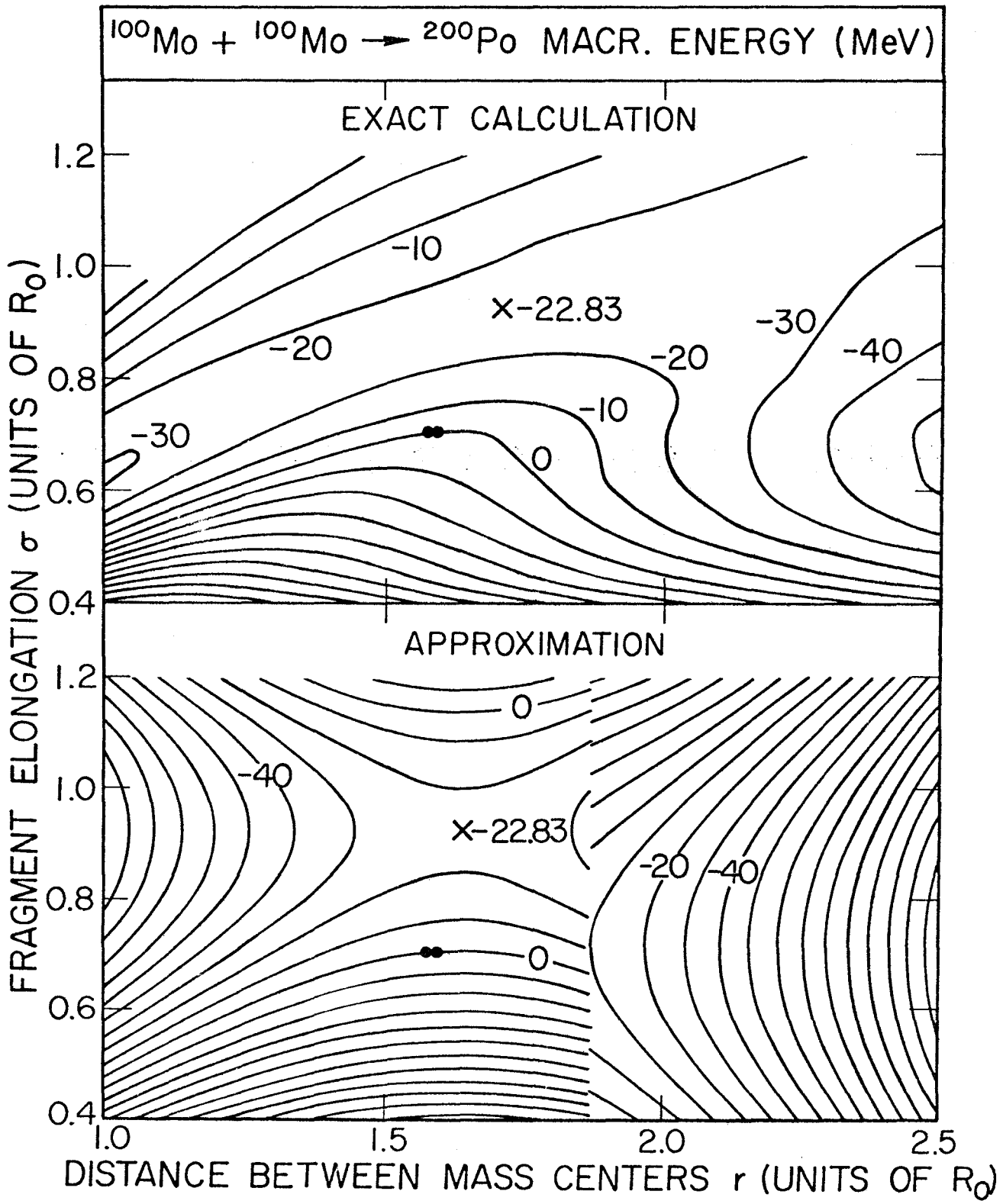
$^{100}Mo + {}^{100}Mo \rightarrow {}^{200}Po$ MACR. ENERGY (MeV)
EXACT CALCULATION
APPROXIMATION
FRAGMENT ELONGATION σ (UNITS OF R_0)
DISTANCE BETWEEN MASS CENTERS r (UNITS OF R_0)
1.2
1.0
0.8
0.6
0.4
1.0
1.5
2.0
2.5
-10
-20
-30
-40
0
X-22.83

Figure 2

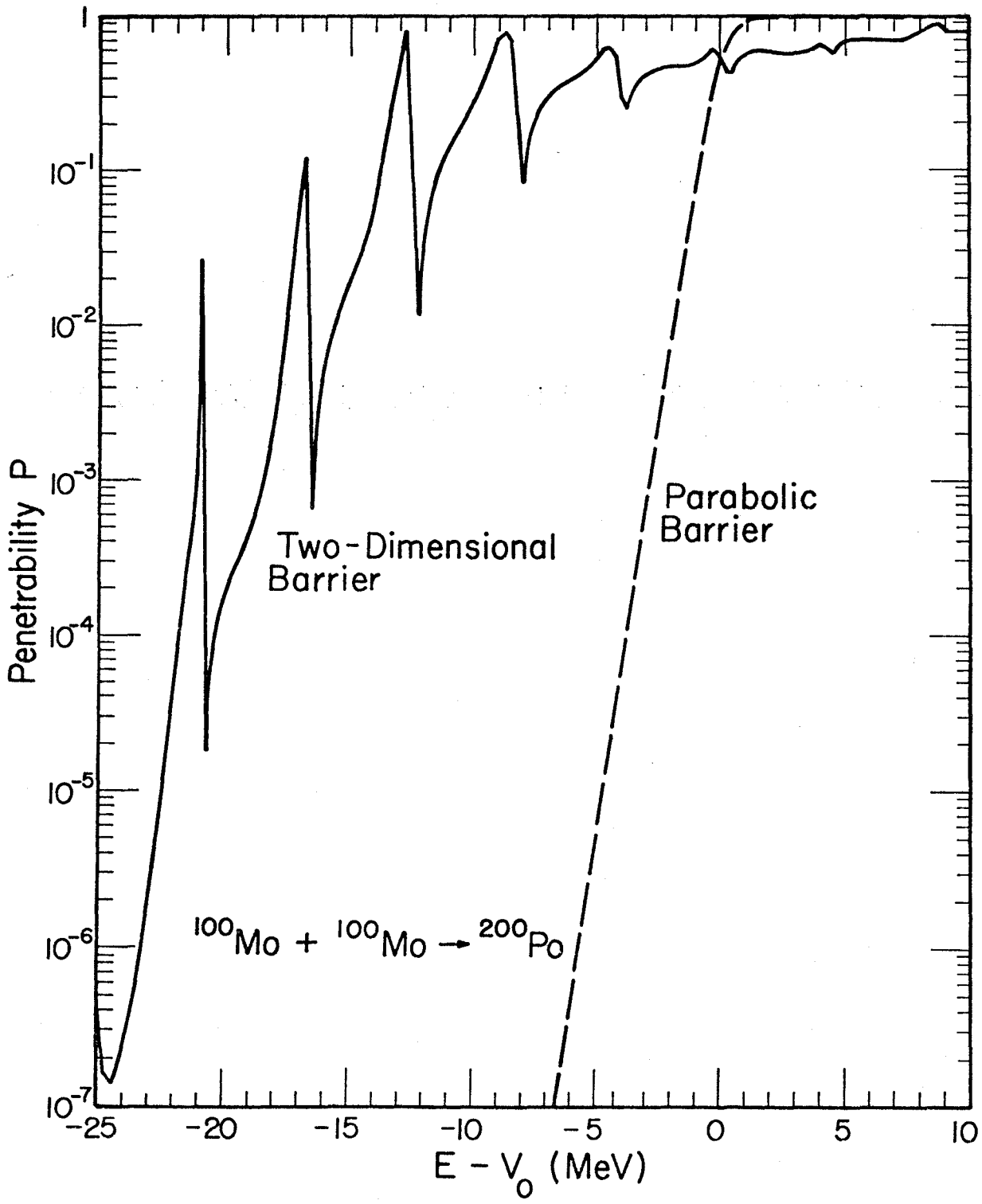
Penetrability P
1
10^{-1}
10^{-2}
10^{-3}
10^{-4}
10^{-5}
10^{-6}
10^{-7}
Two-Dimensional Barrier
Parabolic Barrier
$^{100}Mo + {}^{100}Mo \rightarrow {}^{200}Po$
-25
-20
-15
-10
-5
0
5
10
$E - V_0$ (MeV)

Figure 3